Preparation of mullite-alumina composite by reaction sintering between Algerian kaolin and amorphous aluminum hydroxide

M.L. Bella, M. Hamidouche, Laurent Gremillard

Preparation of mullite-alumina composite by reaction sintering between Algerian kaolin and amorphous aluminum hydroxide

Published in Ceramics International 47 [11] pp. 16208-16220 (2021)
https://doi.org/10.1016/j.ceramint.2021.02.199

M. L. Bella[a,b,*], M. Hamidouche[a,b], Laurent Gremillard[c]

[a] Emerging Materials Research Unit, Ferhat Abbas University of Setif 1, Algeria
[b] Institute of Optics and Precision Mechanics, Ferhat Abbas University of Setif 1, Algeria
[c] Univ Lyon, INSA-Lyon, CNRS, MATEIS UMR 5510, F-69621 Villeurbanne, France
* Corresponding author: amine_bella@hotmail.fr

Abstract

The objective of this work is to obtain a multifunctional ceramic composite material at low cost with improved properties and that can be used in many structural applications like: electrical, refractory support and tribological elements. A mullite-alumina composite were prepared by using Algerian kaolin and amorphous aluminum hydroxide as starting materials. Two mixtures were used by varying the amorphous aluminum hydroxide content 61.5% and 50 wt %. an abundant kaolin has been chosen with a high alumina content and an amorphous alumina trihydrate to lower the temperature of the reaction with the excess of silica in the kaolin. The advantage of adding an amount of amorphous aluminum hydroxide is that it reacts at high temperature with the amorphous phase of silica issue from kaolin. The objective is to increase the amount of the mullite phase formed. When alumina is added in excess, a part will be dispersed in the mullite matrix to form a mullite-alumina composite.

The results revealed that mullite is the major phase and alumina the minor phase in the samples sintered at 1600 °C. At this firing temperature, no silica phases (SiO2) are detected. The microstructure shows a higher aspect ratio of mullite crystals. The addition of alumina reduces the size of mullite grains and their aspect ratio. The density and hardness of the resulting mullite-alumina composites increase with sintering temperature and alumina content.

Keywords

Kaolin, Mullite, Aluminum hydroxide, Mullite-alumina composite

1. Introduction

Kaolin is an abundant clay belonging to the group of phyllosilicates, kaolinite ($Al_2Si_2O_5$) dominates its mineralogical composition. Kaolin is in the form of platelets, which generally have a pseudo-hexagonal crystal shape [1], Kaolin is ‘‘1:1″ clay minerals, their layered structure is formed by a single tetrahedral Si sheet linked by covalently bonded to a single octahedral Al sheet [2]. When kaolin is sintered at a temperature above 1000 °C, it transforms into mullite ($3Al_2O_3{\cdot}2SiO_2$) and cristobalite (SiO_2) [3]. Then, cristobalite transforms into amorphous phase at temperatures above 1400 °C [4].

According to Chen [5], the mechanical properties of sintered kaolin depend on the firing temperature, ie according to its microstructure. Liquid phase sintering is the dominant mechanism during densification of kaolin bodies. The maximums of mechanical strength (180 MPa) and toughness (2 MPa $m^{1/2}$) are obtained for samples sintered between 1300 °C and 1500 °C. The presence of a large amount of vitreous phase appears to be the cause.

Mullite is only the stable crystalline compound in the Al_2O_3/SiO_2 phase diagram under normal atmospheric pressure from room temperature to its melting temperature at 1810 °C [6]. It has interesting properties such as good resistance to thermal shock, high refractory property, low thermal expansion, good creep resistance and good mechanical resistance at high temperatures [[7], [8], [9]].

Torrecillas et al. [7] have investigated the mechanical properties of dense crystalline mullite with their relationship with microstructural features. They found toughness of the order of 2.5 MPa $m^{1/2}$ and mechanical resistances exceeding 250 MPa. For thermal shock resistance, mullite presents a critical temperature difference ΔTc of about 750 °C in the case of soft cooling thermal shock with: Biot number β = 0.3, heat transfer coefficient h = 600 W/m^2 °C and specimen size of (40 × 6 × 4) mm^3 [10].

Also, it is characterized by good chemical stability, and good resistance to wear and friction [11]. For these excellent properties, mullite is widely used as structural and functional ceramic in various applications such as components for electronics, furnace resistance supports, substrates, ball bearings, cylinders and piston rings in automotive engines, …. Researchers have made considerable efforts to synthesize mullite powder and to prepare dense sintered components [12,13]. These processes involve very expensive precursors that can make them unsuitable for industrial production [14]. Synthetic methods using natural clay raw materials, which contain kaolinite, sillimanite, alumina, gibbsite or boehmite are good and cheaper alternatives which have been the subject of much research [3,15,16].

However, mullite formed from natural clays most often contains a high amount of glass phase. A combination between kaolin clay and alumina may be the right solution in this case. Indeed excess alumina can react with the amorphous phase to form additional mullite. The addition of adequate amount of alumina (Al_2O_3) can therefore suppress the amorphous phase and thus increase the amount of mullite in the final material. The decrease of the amount of glassy phase has a positive effect on the mechanical properties of mullite, especially at high temperature.

In this work, three Algerian kaolin are used as source materials to process mullite, referenced respectively as DD1, DD2 and DD3. They are extracted from Djebbel Debbagh, located in the northeast of Algeria. They are considered as a kaolinite clay rich in alumina (41 wt %). This makes it very suitable for the manufacture of structural ceramics based on aluminosilicate compounds.

The formation of mullite prepared by reactive sintering between the three kaolin and an amorphous aluminum hydroxide are studied. In particular, the kinetics of formation of mullite are assessed, as well as, the microstructure development and the Vickers hardness, with respect to the different compositions and sintering conditions.

2. Experimental procedure

2.1. Experimental techniques

The chemical compositions of the raw materials (kaolin and amorphous aluminum hydroxide) were assessed by X-ray fluorescence spectroscopy (Rigaku ZSX Primus IV, Japan). X-ray diffraction (BRUKER D8 Advance with Cu Kα radiation) was used to detect and identify the different phases: 2θ between 5° and 80°, 0.05° step size, exposure 0.08 s per step. XRD was also used to measure the theoretical density of each sample as follows: First, a calibration curve linking the Si/Al molar ratio in mullite and its lattice parameter **a** was established from PDF files [17]. Then Rietveld refinement of XRD-diagrams enabled the determination of both the lattice parameter **a** and the Al2O3/mullite ratio for each material. These two properties were then used to calculate the Si/Al molar ratio in the crystalline phase of each material. On the other hand, the chemical composition of the starting kaolin (Table 2) and the Kaolin/$Al(OH)_3$ ratio of each mixture enabled the calculation of nominal Si/Al molar ratios. Assuming a complete conservation of the aluminum and silicon during processing, it was thus postulated that the missing Si formed an amorphous phase of overall composition SiO_2 and density 2.2 g cm^{-3}, which enabled calculating the absolute density of the obtained materials. Comparison with the observed density allowed to access the relative density and porosity.

The particle size distribution of the starting powders were measured by a laser granulometer (Malvern Mastersizer 2000). The chemical bonds of the phases formed during the firing of amorphous aluminum hydroxide - kaolin mixtures at different temperatures were studied by Fourier transform infrared (FTIR) spectroscopy (JASCO FT/IR-4200 spectrometer), with a smart endurance single bounce diamond, attenuated total reflection (ATR) cell. Spectra in the 4000–600 cm^{-1} range were have obtained by the co-addition of 40 scans with a resolution of 4 cm^{-1}. Differential thermal and thermogravimetric analyzes (DTA and TGA) were carried out in air between ambient and 1400 °C with a heating rate of 10 °C/min using a TA instrument SDT Q 600 V20.9 Build 20 apparatus.

The density of the sintered samples was measured by the Archimedes method using ionized water as the immersion medium.

Vickers hardness (HV) was assessed under ambient conditions using the Vickers indentation method instrumented with a Zwick - Roell ZHU 2.5 device, with a maximum load (F) of 9 N and a 15 s holding time at maximum load. The diagonal of the indents (2a) were measured by optical microscopy (microscope Zeiss Axiovert 40 MAT) and HV was then calculated according to the following relation:

$$H_v = \frac{1.8544 \times F}{2a^2} \qquad (1)$$

The polished samples have been thermally etched, according to the following sintering cycle:

- Rapid rise in temperature (20 °C/min).
- Hold for 30 min at 150 °C below the temperature of sintering.
- Rapid temperature drop (20 °C/min).

The microstructures were examined by scanning electron microscopy (SEM, SUPRA 55VP, Zeiss, Germany).

2.2. Materials

Amorphous aluminum hydroxide $Al(OH)_3$, commercialized by sigma-Aldrich company, was used as a starting powder. Table 1 gives its chemical composition. It has a density of 2.23 g/cm^3 and it has a narrow, monomodal particle size distribution by volume centered on an average grain size of 6 µm (Fig. 1).

Table 1 : Chemical composition of starting alumina tri-hydroxide (wt %).

	Al_2O_3	SiO_2	Na_2O	MgO	P_2O_5	SO_3	Cl	K_2O	CaO	Fe_2O_3	Fire loss (%)
$Al(OH)_3$	72.9	1.15	1.2	1.32	0.01	0.5	0.03	0.04	0.45	0.04	22.36

Table 2 : Chemical composition of starting materials (wt %).

	DD1	DD2	DD3
Al_2O_3	41.9	41.6	40.6
SiO_2	48.8	48.3	46.8
Na_2O	0.05	0.06	0.04
MgO	0.01	/	0.03
P_2O_5	0.01	0.02	0.02
SO_3	0.13	1.33	0.34
Cl	/	0.03	0.04
K_2O	0.01	0.27	0.07
CaO	0.21	0.2	0.37
MnO	/	0.01	2.34
Fe_2O_3	0.04	0.05	0.07
NiO	0.02	0.01	0.11
ZnO	0.01	0.01	0.09
As_2O_3	0.05	0.06	0.06
SrO	/	0.02	/
Fire loss (%)	8.76	8.03	9.02

The three kaolin used in this study are extracted from the mountains of Djebel Debbagh (northeast of Algeria). They are referenced respectively as DD1 of whitish color, the light pinkish color of kaolin referenced DD2 is caused by the presence of alunite [18,19] and DD3 of grayish color because of its content of manganese oxide (MnO). The three types of Kaolin contain in mass, approximately 42% of alumina and 48% of silica. Table 2 gives the average chemical composition of the three Kaolin.

For preparation of the mullite samples by reactive sintering, the three kaolin were ground to a particle size less than 63 µm. Then for each kaolin (DD1, DD2 and DD3) two mixtures with alumina trihydrate were prepared, denoted M1 and M2 according to the compositions mentioned in Table 3.

Table 3 : Compositions for both studied subsystems (Kaolin + aluminum hydroxide) in (% wt).

Mixture composition	M1	M2
Kaolin (%)	38.5	50
$Al(OH)_3$ (%)	61.5	50

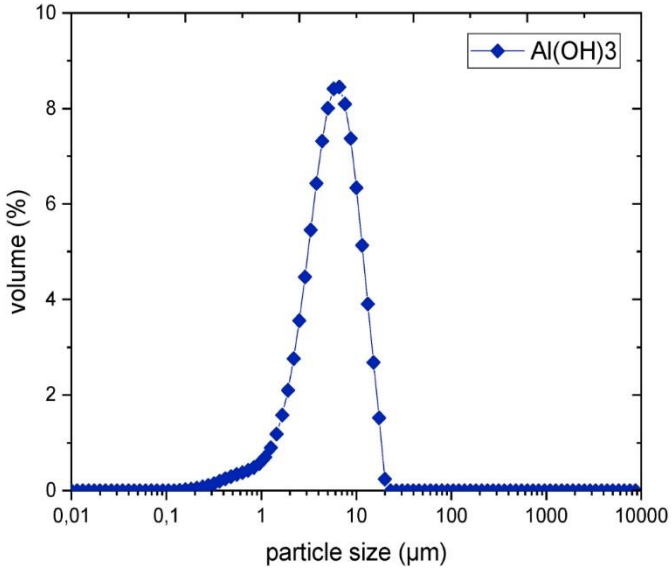

Figure 1 : Particle size distribution by volume of aluminum hydroxide powder used.

According to the stoichiometric equation: adding aluminium tri-hydroxide to kaolinite will lead to the formation of mullite:

$$Al_2Si_2O_5(OH)_4 + 4Al(OH)_3 \rightarrow 3Al_2O_3{\cdot}2SiO_2 + 8H_2O$$

Calculation showed that the mass of the amorphous aluminum hydroxide needed to be add to the kaolin, to have a stoichiometric reaction, is 54.72% by mass. We opted for two additions of $Al(OH)_3$.

- The M1 composition, with 61.5% added $Al(OH)_3$, will give a mullite-alumina composite above the stoichiometry. This will allow all the excess of silica in the kaolin to be consumed.
- The M2 composition, with 50% addition of $Al(OH)_3$, will lead to obtaining a mullite-alumina composite with an excess of silica, ie a composition below the stoichiometry. This will allow a small amount of glassy phase to be in the resulting composite.

The two prepared mixtures were dispersed in ionized water according to the following ratio: 50% of powder mixture/50% of water (in mass).The suspension was ground for 48 h using an attrition grinding mill with alumina balls (Ø ≈ 1.5–2.5 mm). The quantity of balls used was 3 times the mass of the ground powder. The particle size was controlled during grinding until obtaining an average size of 2.5 µm (Fig. 2). Then the suspensions were dried at 110 °C to guarantee their complete drying. Then, the powders were de-agglomerated in a mortar and then sieved to obtain agglomerates of less than 63 µm.

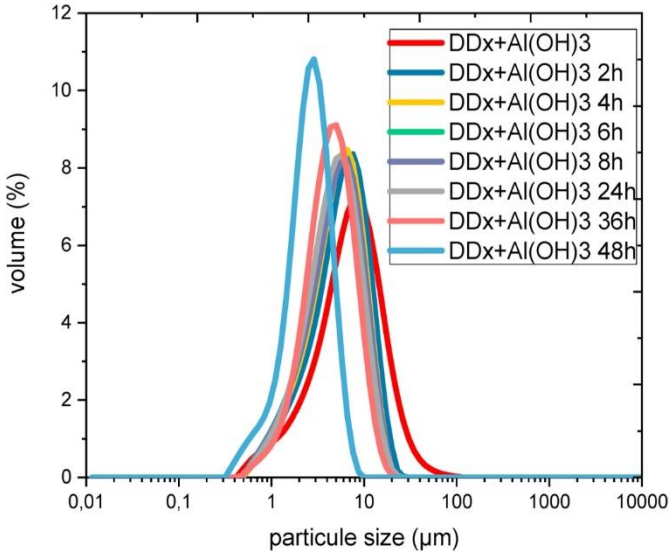

Figure 2 : Particles size distribution of (DDx + aluminum hydroxide) mixtures compositions milled during up to 48 h (the mixtures with the 3 Kaolin and compositions M1 and M2 exhibited identical particle size distributions).

The samples were pressed uniaxially under a pressure of 100 MPa, to cylindrical pellets with a diameter of 25 mm and a thickness of 7.5 mm. To avoid cracking of the pellets, all samples were pre-sintered for 1 h at 600 °C with a low heating rate (1 °C/min). Finally, the pellets were sintered

in air for 5 h at different temperatures (1400 °C, 1500 °C and 1600 °C) using 5 °C/min heating and cooling rates.

The flat faces of the sintered samples were polished using a BUEHLER automet 250 polisher. The polishing was carried out in two stages, the first one is a pre-polishing of the sample with four discs (Φ 250 mm) with diamond suspensions according to the fractions P120 (125 µm) (until the flatness), P220 (68 µm), P600 (30 µm) and P1200 (15 µm) for 3 min for each case. The applied force is 30 N with a rotational speed of the plate of 150 rpm with an opposite direction of rotation (disc relative to the sample) and lubrication with water. In the second step, diamond abrasive suspensions of 6 µm, 3 µm and 1 µm has been used with the same conditions in the first step except for the applied force which is this time 20 N, in addition to the use of appropriate discs. The samples were cleaned in ultrasonic tank with ethanol, after each operation.

3. Results and discussion

3.1. Characterization of starting materials

3.1.1. Amorphous aluminum hydroxide

The DTA-TGA curves of the aluminum hydroxide powder (Fig. 3) show the thermal and thermogravimetric behavior of the amorphous aluminum tri-hydroxide powder.

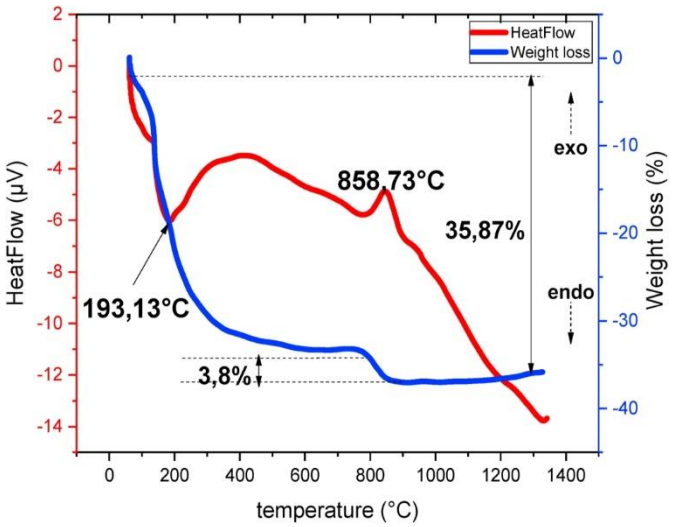

Figure 3. DTA/TGA curves of the aluminum hydroxide raw powder.

The TGA curve for aluminum tri-hydroxide shows a total mass loss of about 35.8%, a rate very close to 34.6% (theoretical value). This loss takes place in two stages according to the following phenomena:
The first mass loss takes place between room temperature and 120 °C. It corresponds to the release of moisture adsorbed on the surface of the powder [20]. The fineness of the amorphous powder explains this behavior, with a large specific surface area, which allowed it to adsorb moisture before use.
The second mass loss is due to zeolite and structural water due to the transformation of amorphous alumina trihydrate into aluminum oxy-hydroxide. This is explained by the large endothermic peak between 100 °C and 500 °C observed on the DTA curve. According to the study of Li et al. [21], amorphous aluminum hydroxide generally undergoes slow dehydration as in our case up to 700 °C. Between 800 °C and 900 °C, the mass loss of 3.8% corresponds to the final de-hydroxylation of aluminum oxy-hydroxide to form γ-Al2O3 transition alumina. This transformation is evidenced by the exothermic peak centered around 860 °C, also observed by other authors [22].
Transition γ-alumina then transforms into θ-Al_2O_3 transition alumina and then into crystalline alumina (α−Al_2O_3) around 1200 °C.

Fig. 4a and b shows the X-ray diffraction diagrams of aluminum hydroxide fired at different temperatures from ambient to 1600 °C. Aluminum tri-hydroxide is completely amorphous between room temperature and 800 °C. This type of aluminum hydroxide has been produced by grinding during for long periods [23]. Characteristic peaks of γ-alumina transition phase are observed between 800 °C and 900 °C. Between 1000 °C and 1100 °C, γ-alumina transforms into another transition alumina (θ phase) and α-Al_2O_3 phase starts to form [24]. Above 1200 °C, only the stable α-Al_2O_3 phase is observed. This sequence of transformations is coherent with the work of Sato et al. [25], who have shown that amorphous aluminum hydroxide transforms with temperatures increasing from ambient to above 1200 °C, as follows:

Amorphous $Al(OH)_3$ → amorphous AlOOH → γ-Al_2O_3 → θ-Al_2O_3 → α-Al_2O_3

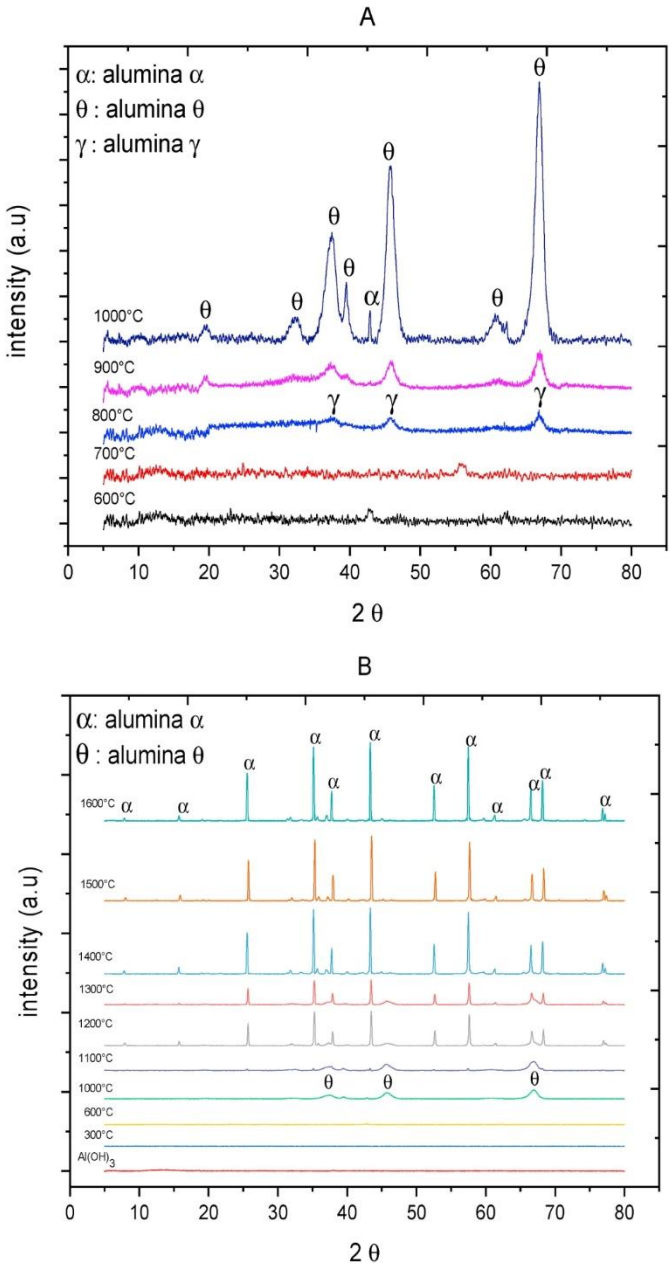

Figure 4. X-ray diffraction pattern of aluminum hydroxide: (A): fired between 600 °C and 1000 °C; (B): fired at different temperatures.

3.1.2. Algerian kaolin: DD1, DD2 and DD3

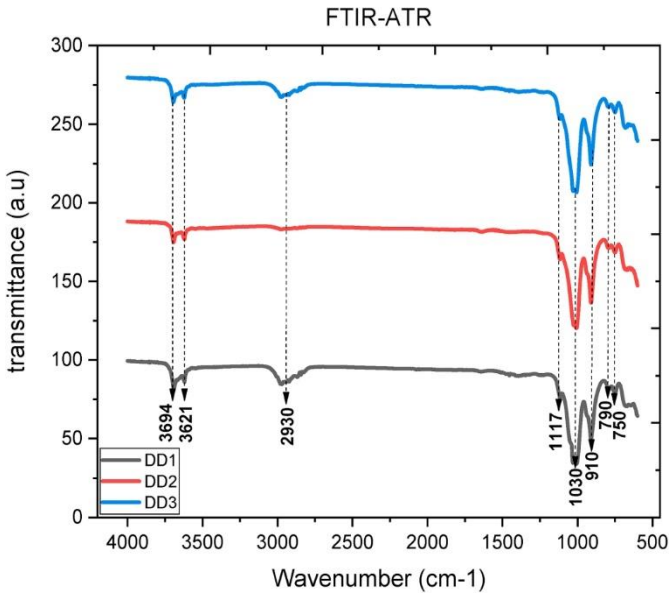

Figure 5. FTIR spectra of the three Algerian kaolin..

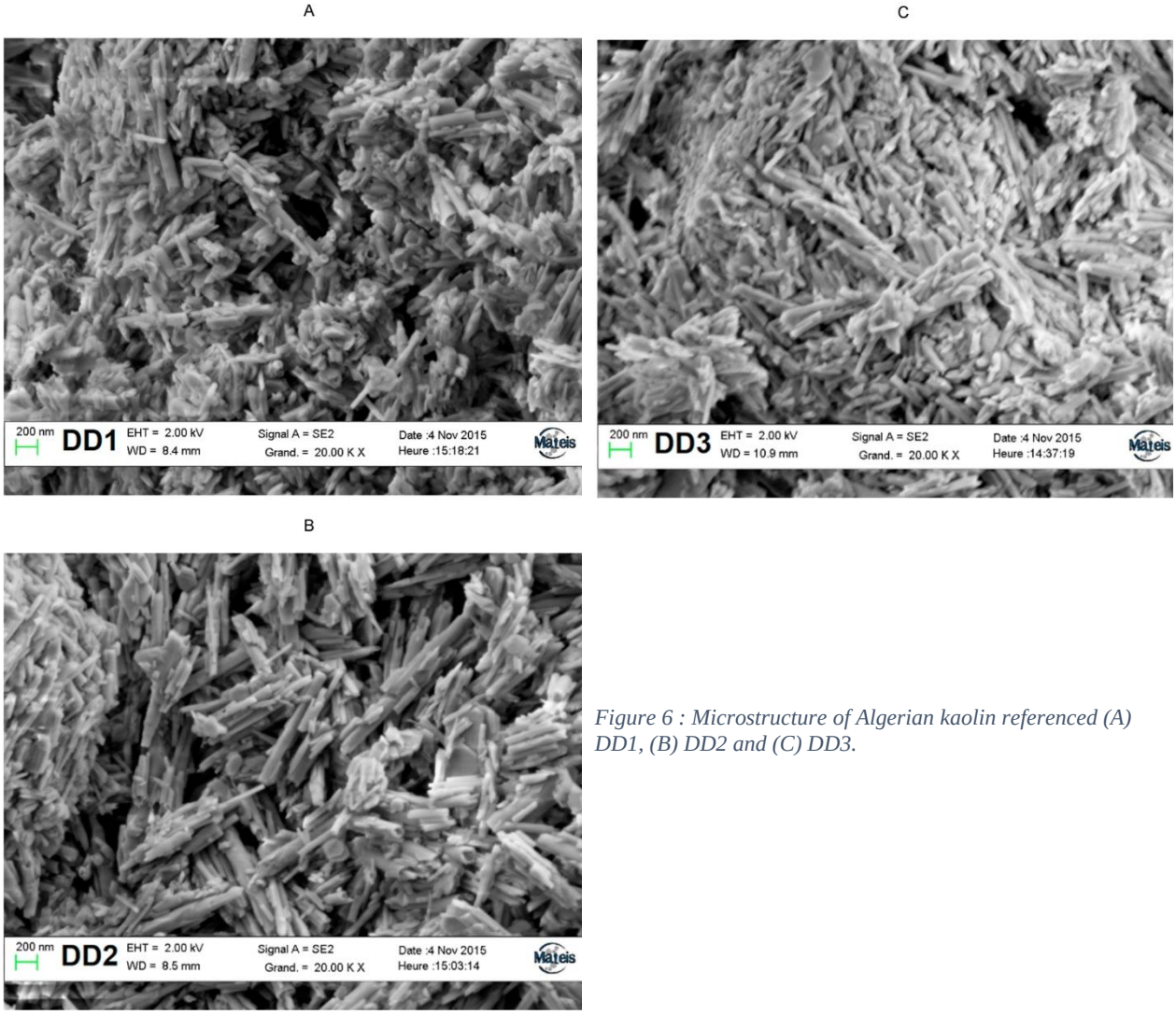

Figure 6 : Microstructure of Algerian kaolin referenced (A) DD1, (B) DD2 and (C) DD3.

Fig. 5 presents the infrared spectra of the different kaolin DD1, DD2 and DD3. A first zone in the spectra corresponds to the high frequency bands located between 3750 cm^{-1} and 3550 cm^{-1}. It is

mainly related to the vibrations of O–H hydroxyls, and particularly to the valence vibrations of the OH groups, which result in the presence of two absorption bands centered on 3694 cm^{-1} (external OH) and 3621 cm^{-1} (internal OH vibration band). A second zone, from 1200 cm^{-1} to 600 cm^{-1}, corresponds to the lower frequencies and relates to the Al–OH, Si–O, Si–O–Si and Si–O–Al bonds. In that zone, the band at 1117 cm^{-1} is attributable to the elongation of the Si–O bond. The asymmetric stretch bond of Si–O – Si and the deformation of the Al–O – H bonds, respectively [[26], [27], [28]] caused the bands observed at 1033 cm^{-1} and 910 cm^{-1}. The bands at 790 cm^{-1} and at 750 cm^{-1}, reduced to an inflection, are typically related to OH translation, which may be due to the presence of halloysite ($2SiO_2 \cdot Al_2O_3 \cdot 4H_2O$) [26]. A low intensity band centered at 2930 cm^{-1} is also observed, attributed to the presence of organic materials.

SEM observation of the three kaolin (Fig. 6) shows that the grains are agglomerates of elongated disordered plates and in form of rolled leaf-shaped grains. The absolute densities measured with a helium pycnometer for the kaolin DD1, DD2, DD3 are respectively 2.56 g/cm^3, 2.56 g/cm^3 and 2.57 g/cm^3.

The DTA curves of the three kaolin (Fig. 7) show the presence of two endothermic peaks. The first peak, located between 47 °C and 65 °C depending on the kaolin, is linked to the removal of water from residual humidity (surface water). This generates a mass loss between 2.5% and 5% for the 3 kaolin. The second endothermic peak is very intense; it appears at a temperature order of 501 °C for DD1, with a mass loss of 14%. In the case of DD2, it is observed at 492 °C, accompanied by a mass loss of 15% and it occurs at 487 °C for kaolin DD3 with a mass loss of 13.7%. This endothermic peak is associated with the release of kaolin structural water to form metakaolinite. In addition to these two endothermic peaks, an endothermic peak is observed, only in the kaolin referenced DD2, at a temperature of 732 °C and associated to a low mass loss of 0.63%.This thermal event is caused by the decomposition of the sulfate present in this type of kaolin [29,30]. The DTA curves show an exothermic peak, without mass loss, between 992.7 °C and 994.6 °C for the 3 kaolin. This peak corresponds to the crystallization of the mullite phase, formed from the transformation of kaolinite.

X-ray diffraction analyses (Fig. 8) show that the different phases present in the kaolin at room temperature are essentially kaolinite ($Al_2Si_2O_5(OH)_4$) and halloysite ($Al_2Si_2O_5(OH)_4–2H_2O$) as major phases and alunite ($K(Al_3(SO_4)_2(OH)_6$) as minor phase. Alunite is present only in the DD2 clay, due to the presence of larger quantities of K_2O and SO_3 in this kaolin (Table 2). In the three kaolin, the two major phases, namely kaolinite and halloysite, transform between 600 °C and 950 °C into amorphous phases, then above 1200 °C into mullite and cristobalite. According to literature [31,32], cristobalite transforms into an amorphous phase at very high temperature (Fig. 8 shows it to happen above 1500 °C), and mullite remains as the only crystalline phase.

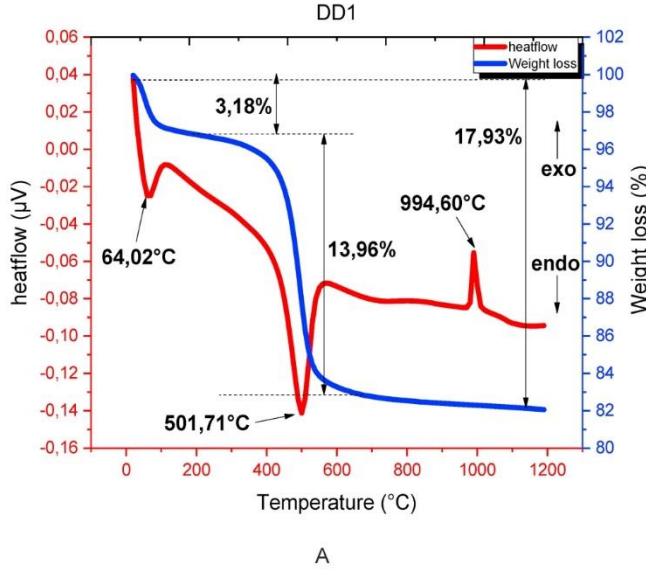

A

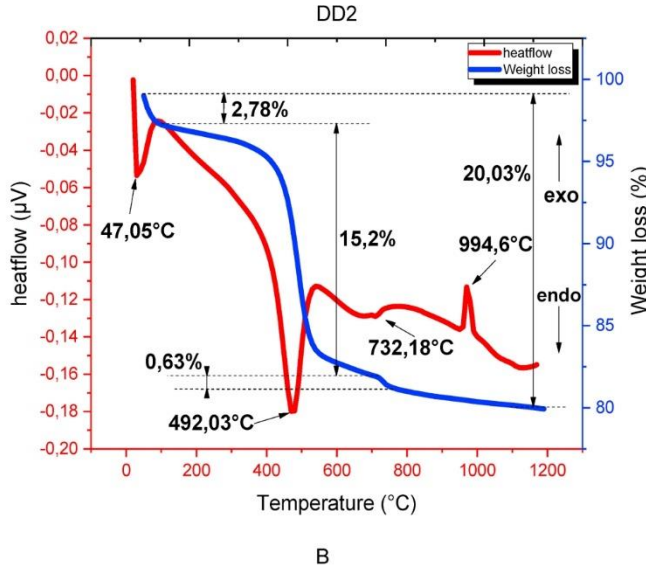

B

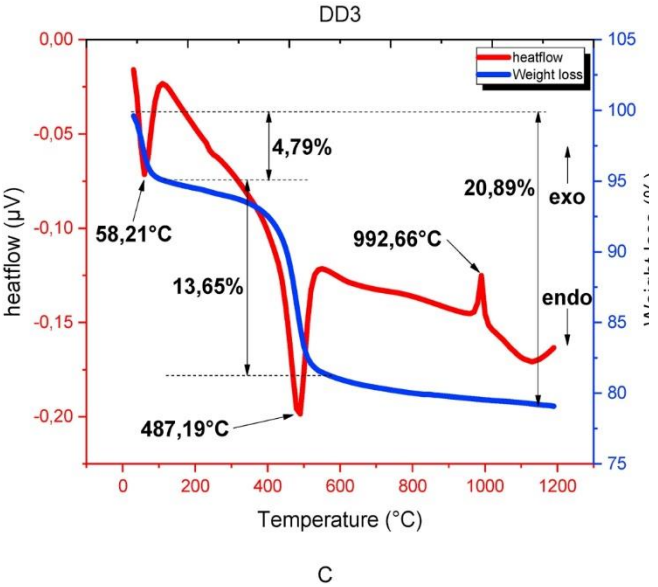

C

Figure 7 : TDA/TG curves of Algerian kaolin heated up to 1200°Cwith rate of 10 °C/min: (A) DD1, (B) DD2, (C) DD3.

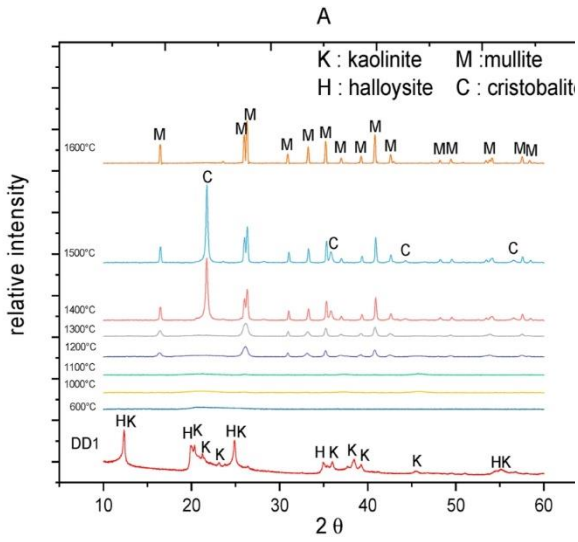

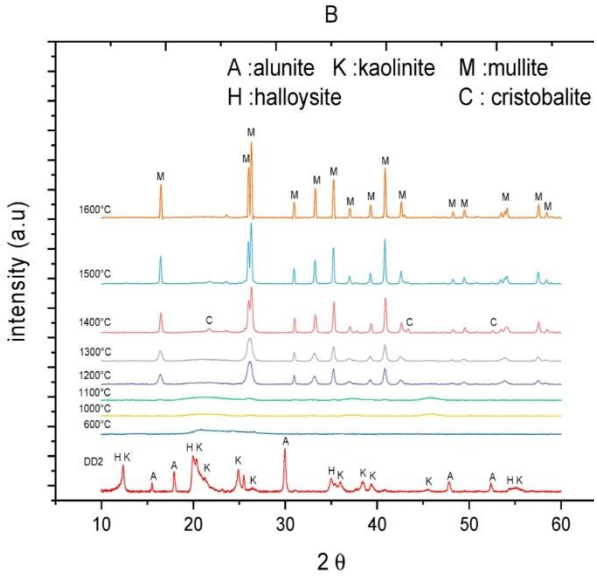

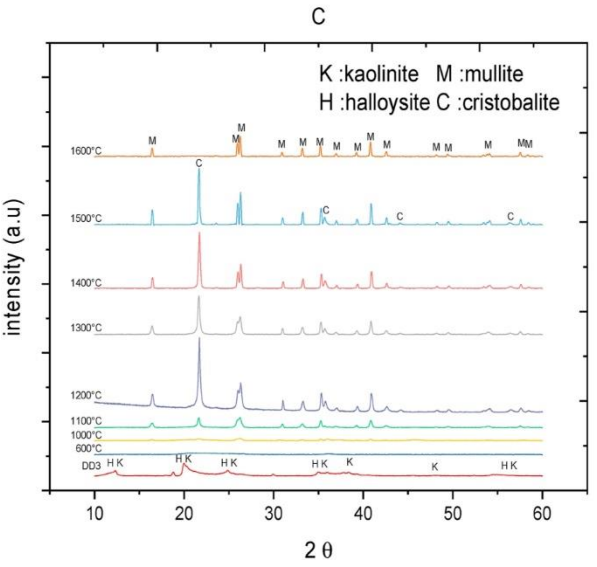

Figure 8 : XRD pattern of the three Algerian kaolin treated at different temperatures (A) DD1,(B) DD2 and (C) DD3.

3.2. Phase evolutions of the mixtures with temperature

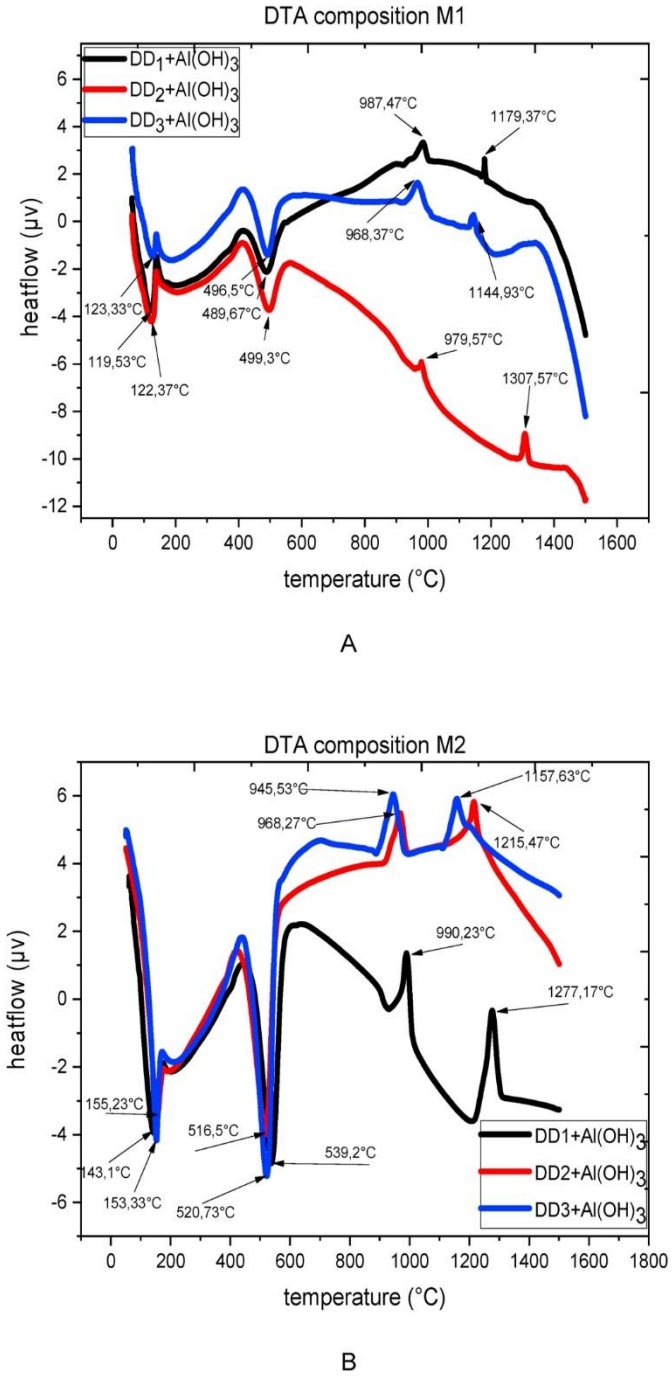

Figure 9. Thermal differential analysis (DTA) of the studied composition mixtures: (A) M1 and (B) M2.

Fig. 9 shows the thermal behavior of compositions mixtures M1 and M2 during a differential thermal analysis (DTA) from room temperature to 1500 °C, conducted in air with a heating rate of 5 °C/min. The DTA curves of figure (9 A and B) show two endothermic peaks for the two mixtures M1 and M2. The first peak is centered around 120 °C for the two mixtures M1 and M2 and corresponds to the departure of surface water from the two powders mixes (kaolin + tri-hydrated amorphous alumina) and zeolitic water located between the sheets of kaolinite of the three kaolin. The second, very intense, endothermic peak is observed at 500 °C for the M1 mixtures and from at 520 °C for the M2 mixtures, and corresponds to the de-hydroxylation of kaolinite [33]. This second endothermic peak is caused by the elimination of structural water by a diffusion mechanism, which results in the formation of amorphous metakaolin, which only crystallizes at higher temperatures. Two exothermic peaks are also observed for the two compositions. The first peak lays between 940 °C and 990 °C, depending on the mixture and on the kaolin nature. This peak, associated to the

formation of mullite from metakaolin, appears at temperatures below to those when kaolin is alone (992 °C). The presence of the transition alumina phases (gamma and theta) facilitates the nucleation of the mullite crystals. The second exothermic peak, between 1150 °C and 1300 °C, is observed for the six mixtures (kaolin + alumina trihydrate). It corresponds to the formation of a secondary mullite phase from the reaction between θ-alumina, formed from amorphous aluminum hydroxide and excess silica from kaolin. This result agrees with those found by other authors [32,34,35].

3.3. Sintered materials

3.3.1. Shrinkage kinetics

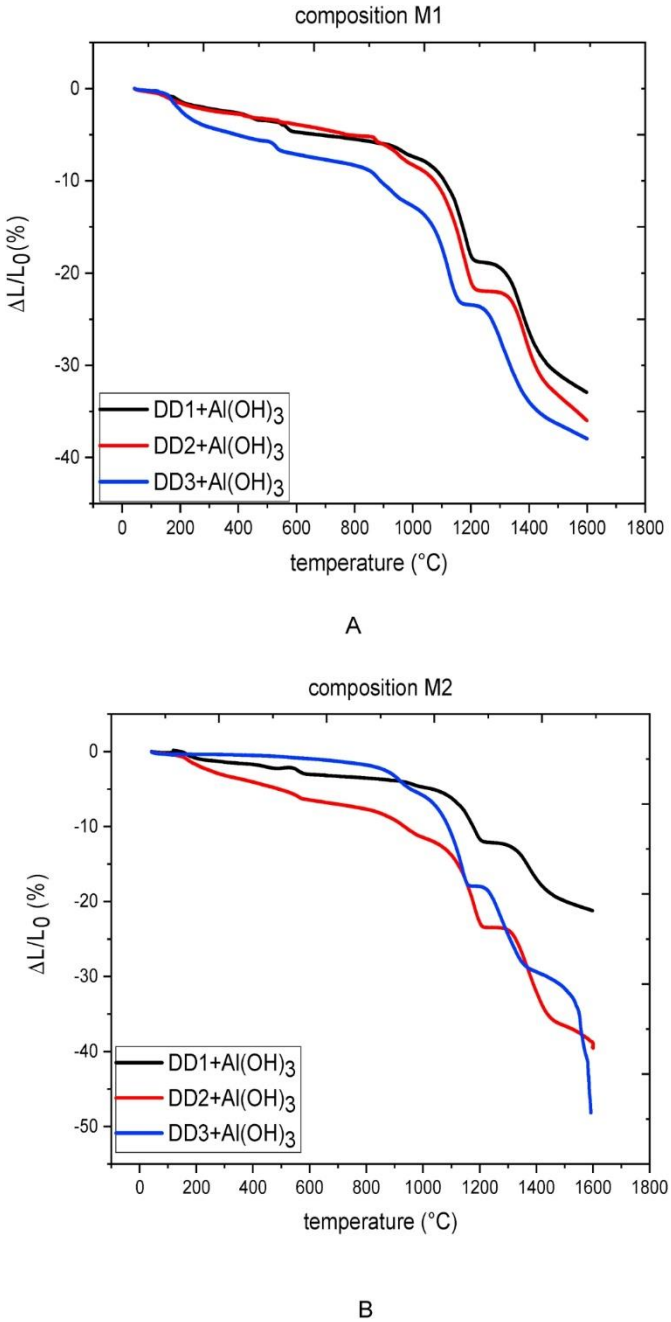

Figure 10 : Shrinkage curves of the green compact for compositions: (A) M1 and (B) M2.

Fig. 10 shows the shrinkage curves as a function of firing temperature, for the six mixtures, from room temperature up to 1600 °C with a heating rate of 5 °C/min. The first shrinkage takes place between 120 °C and 220 °C, where aluminum hydroxide and kaolin release surface water. Between 500 °C and 600 °C, kaolinite undergoes de-hydroxylation and transforms into metakaolin, which causes the second shrinkage. To this effect, the hydroxyl groups are removed from the intermediate layer between the layers of Si–O and Al–O in the kaolinite crystals [4]. The third shrinkage, observed between 850 °C and 1000 °C, corresponds to the transformation of metakaolinite into so-

called primary mullite [36]. A fourth significant shrinkage extends from 1020 °C to 1220 °C, and is caused by the transformations of transition alumina into α-alumina, the most stable alumina, which has the highest density. In this temperature range, the excess of silica originating from the initial kaolin is still present. The fifth and final shrinkage begins beyond 1200 °C until the end of the heating cycle. This shrinkage is associated with the reaction of the silica phase with the θ-alumina present in the mixtures up to 1300 °C.
This second mullite was nucleated in the transitional vitreous liquid phase by dissolution of the alumina. The grains of the secondary mullite present a different structure (acicular) and grains size smaller than those of the primary mullite formed by kaolin transformation [32].

The samples shrinkage observed above 1400 °C is due to the sintering start of the composite material formed.

3.3.2. Microstructure and phase analysis

Table 4 groups the results of the apparent density for the different compositions, as a function of the sintering temperature. The values of the composition M1 are greater than those of composition M2, because the first composition contains more alumina. The densification-taking place at temperatures below 1600 °C is due to the small particle size of the mixture of starting powders because it is ground for 48 h. This large specific surface area reduces the diffusion distances, which increases the driving force of the sintering as found by other authors [33].

Table 4 : Apparent density of all materials.

	Composition M1 Apparent density (g/cm^3)			Composition M2 Apparent density (g/cm^3)		
sintering temperature	**1400°C**	**1500°C**	**1600°C**	**1400°C**	**1500°C**	**1600°C**
DD_1 + $Al(OH)_3$	2.97±0.02	3.06±0.05	3.07±0.01	2.95±0.04	3.03±0.04	2.98±0.02
DD_2 + $Al(OH)_3$	3±0.06	3.10±0.05	3.10±0.01	3.05±0.05	3.07±0.02	3.00±0.02
DD_3 + $Al(OH)_3$	3.06±0.04	3.10±0.01	3.06±0.02	3.03±0.03	3.02±0.01	2.98±0.01

The low density observed for the mixtures based on DD1 kaolin sintered at 1400 °C. is due to the presence of the compounds before the reaction (silica, alumina). At this temperature, the cristobalite, with the impurities of the kaolin, transforms into a liquid phase. This proves the non-completion of the silica-alumina reaction but also prevents the diffusion to accelerate the sintering. These results confirms those obtained by Chantale Njiomou Djangang et al. [37].

The density increases with increasing of sintering temperature for the two compositions, due to porosity closure. In all cases, the density is lower than the absolute density of the mullite (3.17 g·cm^{-3}), hinting to remaining porosity, all the more that the presence of alumina dispersoids should increase the density.

Fig. 11 shows the relative density and apparent porosity of the alumina mullite composite sintered at different temperatures. It is observed that composition M1 samples achieved relative densities of 93 %–97.8% in the specimens sintered at 1600 °C, and 96 %–98% in composition M2, in the specimens sintered at 1500 °C, on the other hand, relative densities decrease to 95 %–96% in samples sintered at 1600 °C in composition M2. In composition M1, the maximum value of the relative density is measured for the compound DD2 + Al $(OH)_3$ (~97.8%). In the composition M2 the maximum value is found for both compounds DD1 + Al $(OH)_3$ and DD2 + Al(OH)3 (~98%). This is due to the significant mullitization rate recorded for these two compounds. On the other hand, the compounds containing kaolin referenced DD3 systematically present the lowest relative density in the six. Indeed, DD3 contains much more volatile material and impurity compared to the other two kaolin, which creates residual porosity that may not be completely removed during the sintering process.

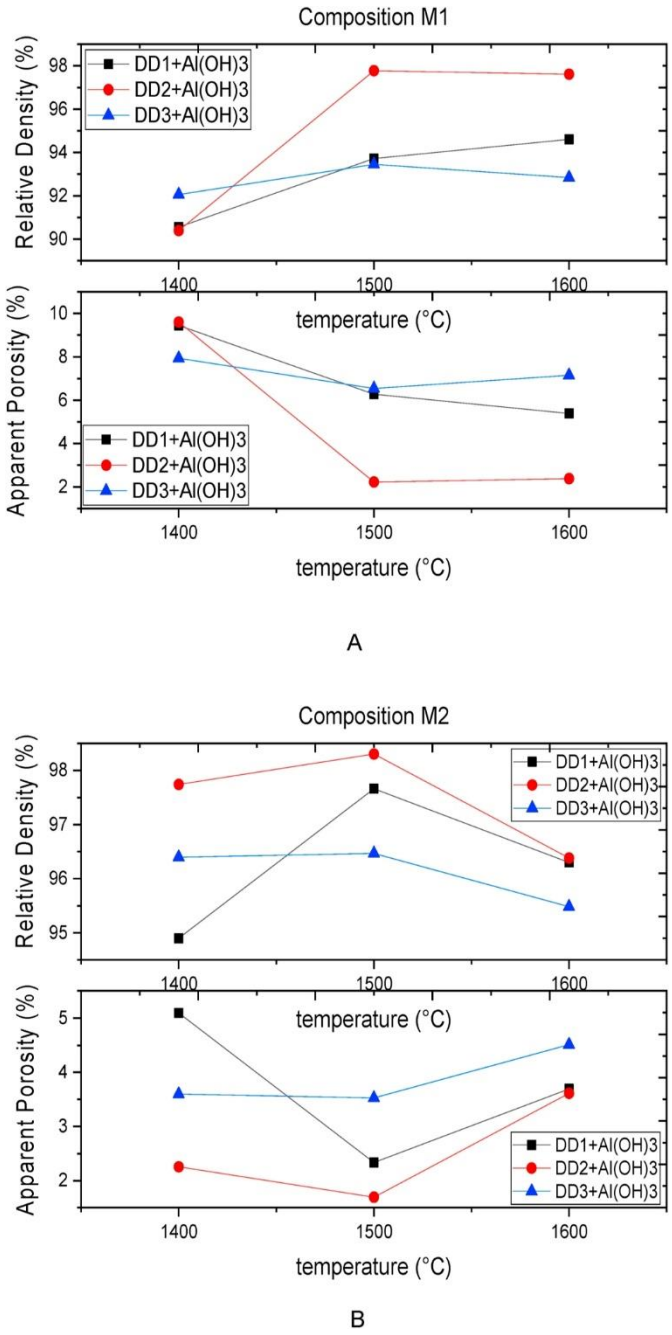

Figure 11 : Relative density and apparent porosity of compositions: (A) M1 and (B) M2.

The apparent porosity in compound M1 decreases with the increase in the sintering temperature. On the other hand, in the composition M2, it is observed that there is a slight increase in porosity and decrease in relative densities between 1500 °C and 1600 °C caused by the presence of much more of the amorphous phase around the grain boundaries compared to composition M1 that contains more excess alumina and less kaolin than composition M2.

The XRD diagrams of the mixtures M1 and M2 for the three types of kaolin, sintered for 5 h at 1400 °C, 1500 °C and 1600 °C, are gathered in Fig. 12. Mullite is the predominant main phase, and no cristobalite is detected (at these temperatures, cristobalite became amorphous and then reacted with alumina to form secondary mullite). Primary mullite results from the transformation of kaolinite while secondary mullite results from the reaction between alumina and the excess of silica in kaolin. The later one is formed by a mechanism of dissolution precipitation through the vitreous phase as mentioned also by other authors [38]. In the case of the sample referenced M2-DD1, no trace of Al2O3 nor any another phase is detected apart from the mullite. All other mixtures contain α-Al2O3 up to 1600 °C, due to the excess of Al2O3 added and which could not react once the amorphous phase was entirely consumed in the reaction.

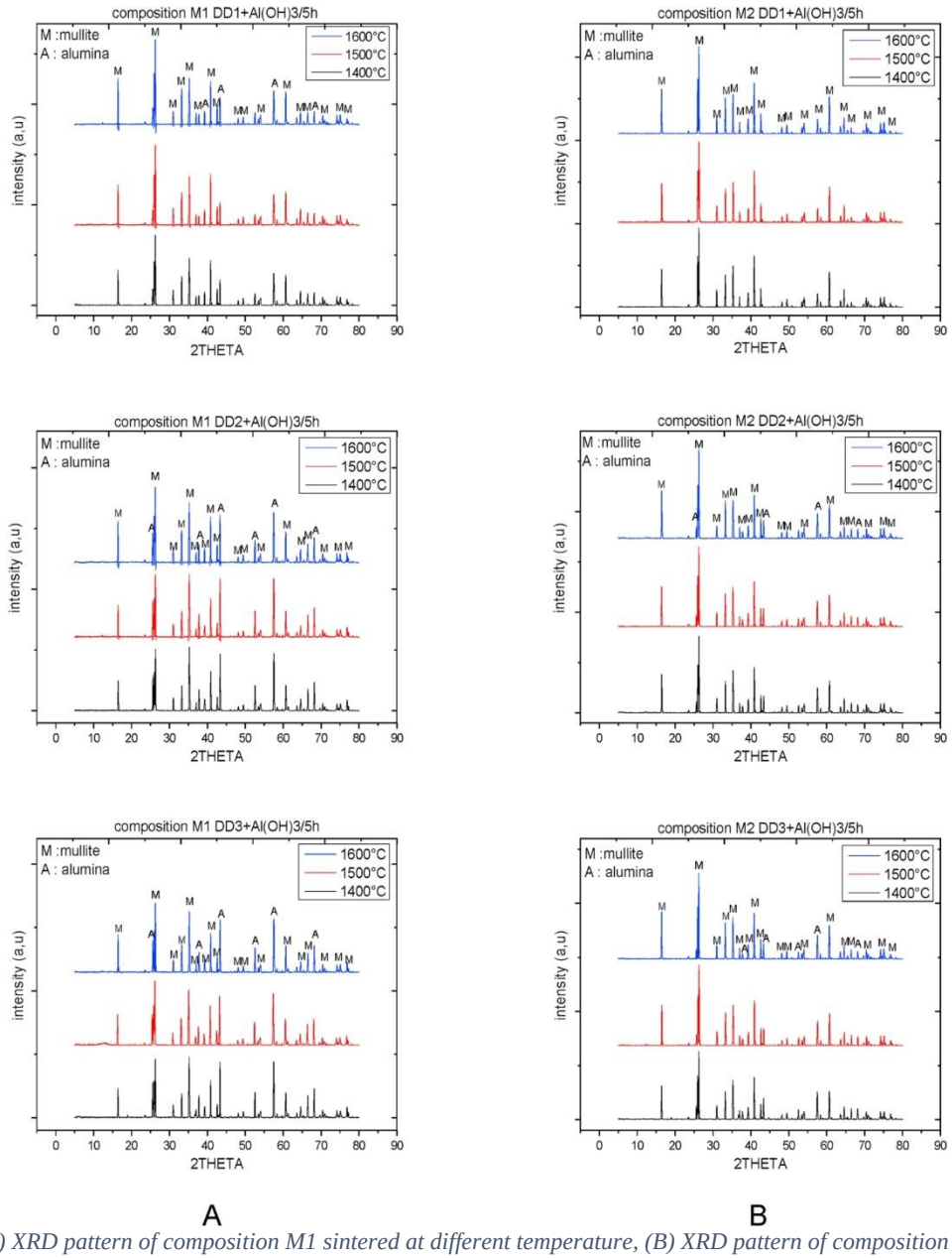

Figure 12 : (A) XRD pattern of composition M1 sintered at different temperature, (B) XRD pattern of composition M2 sintered at different temperature.

For the different compositions, increasing the sintering temperature accelerates the formation of secondary mullite. Indeed, from 1500 °C, the reaction between alumina-vitreous silica of kaolin seems to be complete. The fine size of the alumina grains combined with the presence of impurities in the starting kaolin, promotes the reduction of the viscosity of the glassy phase at these temperatures. This promotes the reaction of alumina with the glassy phase to form more secondary mullite, resulting in total crystallization of the compound.

Fig. 13 displays the results of the quantification of the secondary mullite formation in M1 and M2 mixtures during thermal treatment, measured by the Rietveld refinement quantitative phase analysis. In M1 composition, about 40% of the mullite formation takes place from 1400 °C. On the other hand, at the same temperature the formed mullite reaches a little more than 80% in M2 composition. At this temperature the amorphous phase has not fully reacted with the excess alumina.

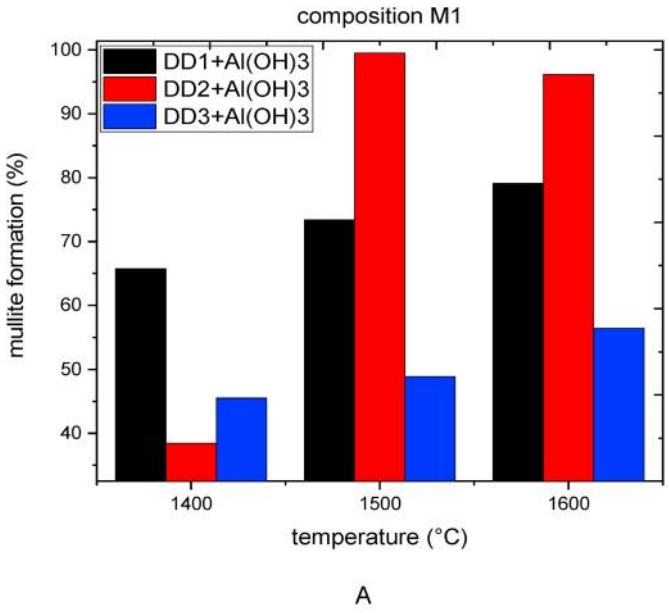

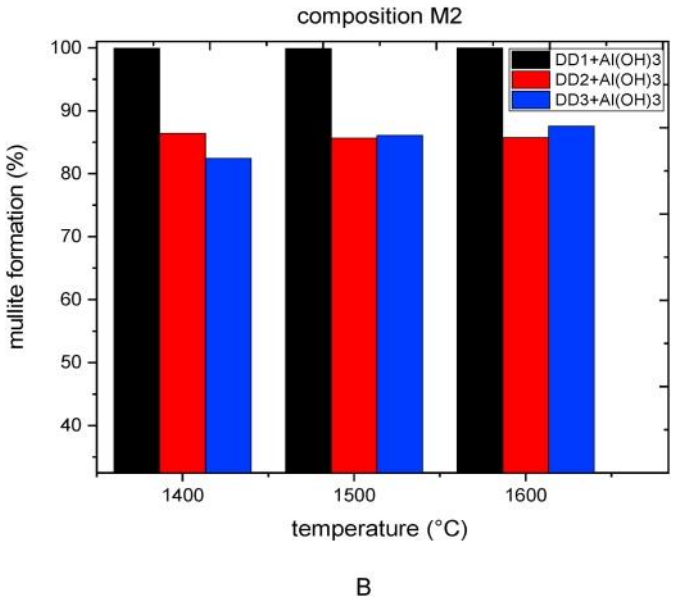

Figure 13 : Mullite formation of composition: (A) M1 and (B) M2 during thermal treatments.

It's noted that from 1500 °C, the formation of mullite increases slowly. It is observed that the formation of mullite in the M1 composition reaches a little more than 99% of mullite in the compound DD2 + $Al(OH)_3$. The M2 composition has recorded a total mullitization of the compound DD1 + $Al(OH)_3$ at a temperature of 1600 °C for 5 h of sintering. At high temperature, the present alumina has been completely dissolved in the amorphous phase for the benefit of the formation of secondary mullite. it is noted that there is a difference in the mullite quantity formed for the three kaolins DD1, DD2 and DD3 in composition M1, compared to composition M2. The impurities present differently in each kaolin facilitate the formation of the liquid vitreous phase from the silica amount of each kaolin. In the composition M1, the alumina amount is in excess, so its dissolution in the liquid phase will be more difficult. Therefore, the precipitation of the mullite will be less.

Fig. 14, Fig. 15 show the microstructures, obtained by SEM, of mixtures (kaolins - alumina) sintered respectively at 1500 °C and 1600 °C for 5 h. The morphology of the microstructures does not present significant differences between the two mixtures M1 and M2. A high porosity is observed for all sintered mixtures at different temperatures.

In the structures, three distinct phases are observed, namely:

- A matrix of secondary mullite grains with acicular form and small grain size (<1 μm), resulting from the reaction of kaolin silica and alumina. They are around 100 nm–200 nm in the case of mixtures M1 and M2 combined with DD1 and DD2. The reaction between alumina and the vitreous phase generally takes place by a dissolution-diffusion-precipitation mechanism. Kaolins containing more K_2O and MnO will accelerate the transformation of cristobalite into the liquid phase and reduce its viscosity. It will lower the temperature of the dissolution and diffusion mechanism and allow the secondary mullite to precipitate at temperatures below. it is observed in the XRD diagrams (Fig. 12) that the cristobalite has not even had time to form since. Malou et al. [39] have shown that the dissolution of alumina in the vitreous phase increases until the nucleation of the mullite then its crystallization. The rapid formation of mullite traps alumina particles and pores which inhibits densification of the composite. The equiaxial form of secondary mullite is caused by the presence of a large amount of alumina.
- Large primary mullite crystals of very elongated shape formed from the final crystallization of kaolinite. They are randomly oriented and uniformly dispersed in the matrix of secondary mullite grains. M.A. Sainz et al. [40] found that the compositions of the primary and secondary mullites vary significantly according to the Al_2O_3–SiO_2 diagram. Secondary mullite is richer in alumina (74.1%) than primary mullite (71.7%).
- Isotropic Alumina grains of a few micrometers dispersed in the mullitic matrix. This alumina phase comes from the excess of the alumina addition, which did not react with the kaolin silica. For the two mixtures M1 and M2 combined with DD1 and DD2, the compositions are not stoichiometric. This finding is confirmed by the spectra of analysis by X-ray diffraction.

The structure of the M1 mixtures of kaolin DD3 led to a larger grain size. This growth of the crystallites could be caused by the incorporation into the mullite of Mn^{4+} cations, present as significant impurity in the kaolin DD3, by substitution for Al^{3+} and Si^{4+} [41].

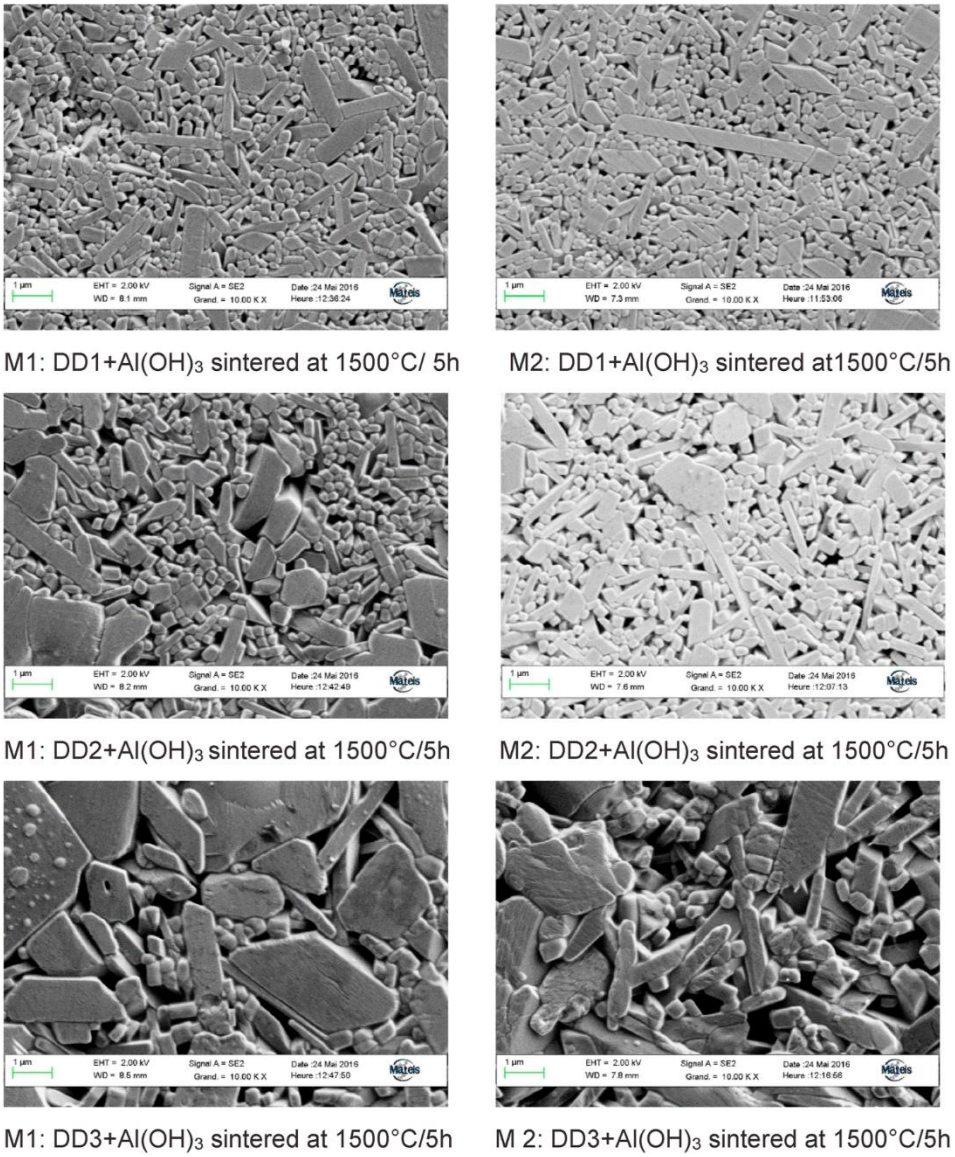

Figure 14 : SEM micrographs samples of the M1 and M2 compositions sintered at 1500 °C during 5 h.

Mullitization occurs from the alumina - silica phase by nucleation and growth due to a reaction between alumina from aluminum hydroxide and amorphous silica from kaolin. The growth rate is controlled by the dissolution of Al_2O_3 in SiO_2. At high temperatures, nucleated mullite will grow at the interface between Al2O3 and SiO2 particles by diffusion of Al^{3+} and Si^{4+} via a crystal lattice. Rapid dissolution of alumina in the amorphous siliceous phase promotes homogeneous nucleation and growth of mullite within the residual vitreous phase [42]. The mixture M1 combined with DD3 (with an excess of alumina) confirms this mechanism. Indeed, some intragranular alumina grains remained trapped in clusters of formed secondary mullite.

The presence of 2.34% MnO promotes sintering in the liquid phase (small amount) in the case of the M2 mixture (less alumina) made from DD3 and sintered at 1600 °C for 5 h.

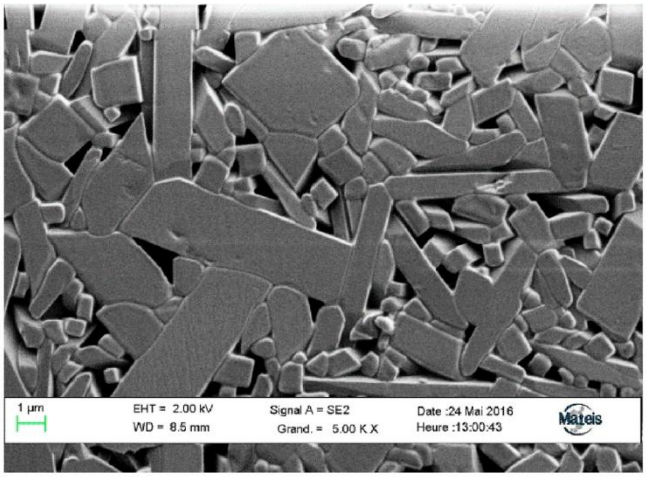

M2: DD1+Al(OH)$_3$ sintered at 1600°C/5h

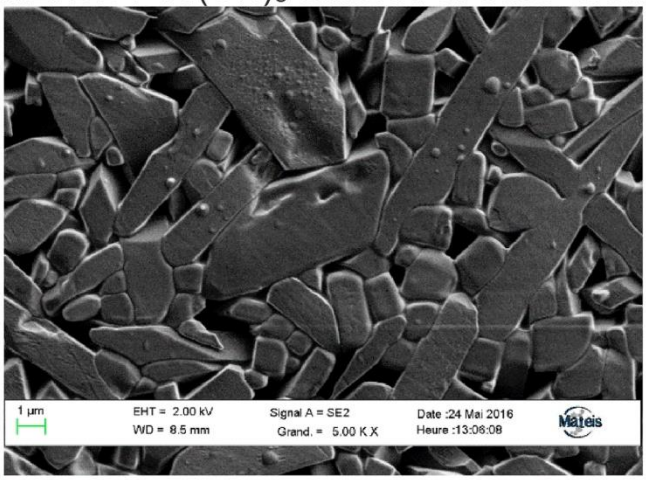

M2: DD2+Al(OH)$_3$ sintered at1600°C/5h

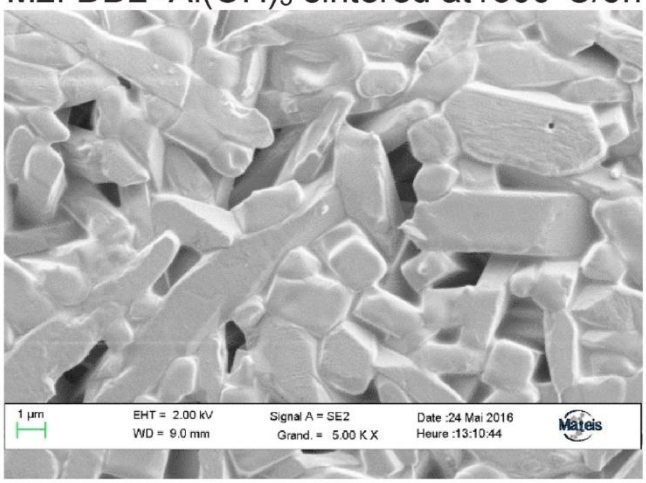

M2: DD3 + Al(OH)$_3$ sintered at 1600°C/5h

Figure 15 : SEM micrographs samples sintered at 1600 °C during 5 h.

3.3.3. Vickers hardness

The average values of the measured hardness of M1 and M2 compositions shown in Table 5, indicate that the hardness values increase with increasing sintering temperature. The studied mullite-alumina composites have higher hardness in comparison with mullite ceramics, which is about 11.3 GPa [43], the presence of the alumina phase increases hardness. These values are in the same order as those found by P.G. De la Iglesia et al. [44].

A sintering temperature of 1400 °C allows the complete reaction between the alumina and the excess silica kaolin. Beyond 1400 °C temperature, sample densification begins to take place. The Compounds sintered at 1600 °C lead to better densification with anisotropic grain growth which

increases the hardness of the composite (alumina-mullite) [45]. The high content of alumina in M1 compositions leads to higher hardness than in M2 composition.

Table 5 : Vickers Hardness of all materials.

	M1 Composition Vickers Hardness (GPa)			M2 Composition Vickers Hardness (GPa)		
Sintering temperature	**1400 °C**	**1500 °C**	**1600 °C**	**1400 °C**	**1500 °C**	**1600 °C**
DD_1 + $Al(OH)_3$	7.49±0.75	13.82±1.12	15.41±0.92	6.58±0.51	11.41±0.92	12.57±0.82
DD_2 + $Al(OH)_3$	9.30±0.28	12.88±0.69	14.84±1.85	9.52±0.71	11.61±0.91	12.02±0.68
DD_3 + $Al(OH)_3$	7.73±1.52	11.23±1.59	12.04±1.13	9.01±0.95	10.01±1.78	10.89±0.42

4. Conclusions

In the present investigation, a composite consisting of mullite and corundum crystals has been prepared by reaction sintering of mixtures of 38.46 wt % Algerian kaolin; 61.54 wt % amorphous aluminum hydroxide powder and 50:50 Algerian kaolin/amorphous aluminum hydroxide at three different temperatures of 1400 °C, 1500 °C and 1600 °C. At 1400 °C, very little densification occurs. At 1500 °C, the densification improves much better, but needle shaped mullite nucleated at this temperature and it grew and crystallized very well at 1600 °C. After formation of mullite by the reactions of alumina and amorphous silica, the excess alumina recrystallized as corundum crystals. The disadvantage is its relatively low density and consequently low strength. Fully dense mullite specimens are thus difficult to prepare by using the process employed in the present study. On the other hand, the advantage of this process is its economic feasibility, the pellet of mullite developed in the present study will be highly suitable for manufacturing ceramic disks for faucet cartridges.

Declaration of Competing Interest

The authors declare that they have no known competing financial interests or personal relationships that could have appeared to influence the work reported in this paper.

Acknowledgements

The authors would like to thank Innovation Fund, Denmark for the financial support of this study under the framework of SYNFUEL (sustainable synthetic fuels from biomass gasification and electrolysis) project (File No. 4106-00006B).

References

1. F. Paul, G. Millot, Géologie des Argiles, altérations, sédimentologie, géochimie, vol. 47, Masson, Paris (1964), pp. 387-388, Norois
2. A. Mikowski, P. Soares, F. Wypych, J.E.F.C. Gardolinski, C.M. Lepienski, **Mechanical properties of kaolinite 'macro-crystals',** Philos. Mag. A, 87 (2007), pp. 4445-4459
3. J.A. Pask, A.P. Tomsia, **Formation of mullite from sol-gel mixtures and kaolinite,** J. Am. Ceram. Soc., 74 (1991), pp. 2367-2373
4. C.Y. Chen, G.S. Lan, W.H. Tuan, **Microstructural evolution of mullite during the sintering of kaolin powder compacts,** Ceram. Int., 26 (2000), pp. 715-720
5. C.Y. Chen, W.H. Tuan, **The processing of kaolin powder compact,** Ceram. Int., 27 (2001), pp. 795-800
6. Y. Li, K.A. Khor, **A study of processing parameters in thermal-sprayed alumina and zircon mixtures,** J. Therm. Spray Technol., 11 (2) (2002), pp. 156-194

7. R. Torrecillas, G. Fantozzi, S. De Aza, J.S. Moya, **Thermomechanical behavior of mullite,** Acta Mater., 45 (3) (1997), pp. 897-906
8. T.I. Mah, K.S. Mazdiyasni, **Mechanical properties of mullite,** J. Am. Ceram. Soc., 66 (1983), pp. 699-703
9. H. Schneider, J. Schreuer, B. Hildmann, **Structure and properties of mullite - a review,** J. Eur. Ceram. Soc., 28 (2008), pp. 329-344
10. M. Hamidouche, N. Bouaouadja, C. Olagnon, G. Fantozzi, **Thermal shock behaviour of mullite ceramic,** Ceram. Int., 29 (2003), pp. 599-609
11. T. Senda, J. Drennan, R. McPherson, **Sliding wear of oxide ceramics at elevated temperatures,** J. Am. Ceram. Soc., 78 (1995), pp. 3018-3025
12. M.D. Sacks, H. Lee, J.A. Pask, **A Review of Powder Preparation Methods and Densification Procedures for Fabricating High Density Mullite**, *In* S. Somiya, R.F. Davis, J.A. Pask (Eds.), Ceramic Transaction, vol. 6, American Ceramic Society, Westerville, OH (1990), pp. 167-207, Mullite and Mullite Matrix Composites
13. D. Amutharani, F.D. Gnanam, **Low temperature pressure less sintering of sol–gel derived mullite,** Mater. Sci. Eng., A264 (1999), pp. 254-261
14. W.E. Lee, W.M. Rainforth, **Ceramic Microstructures, Property Control by Processing,** Chapman and Hall, London, UK (1994), pp. 299-311
15. M. Kolli, M. Hamidouche, G. Fantozzi, J. Chevalier, **Elaboration and characterization of a refractory based on Algerian kaolin,** Ceram. Int., 33 (2007), pp. 1435-1443
16. H. Belhouchet, M. Hamidouche, N. Bouaouadja, V. Garnier, G. Fantozzi, **Kinetics of mullite formation in zircon and boehmite mixture,** Ann. Chimie - Sci. Mater., 35 (1) (2010), pp. 17-25
17. PDF-2 2000 database (ICDD): PDF files # 73-1253, 73-1389, 74-2419, 79–1275, 79-1276, 79-1450 to 79-1458, 82-37, 83-1881, 84-1205, 85-1460, 82-1237.
18. M. Ç Karakaya, N. Karakaya, A. Temel, F. Yavuz, **Mineralogical and geochemical properties and genesis of kaolin and alunite deposits SE of Aksaray (Central Turkey),** Appl. Geochem., 124 (2021) 104830
19. H. Mutlu, K. Sariiz, S. Kadir, **Geochemistry and origin of the Şaphane alunite deposit, Western Anatolia, Turkey,** Ore Geol. Rev., 26 (2005), pp. 39-50
20. X. Xu, Y. Liu, Z. Li, Z. Lv, J. Song, M. He, Q. Wang, L. Yan, Z. Li, **Thermal study of boehmite nanofibers with controlled particle size,** J. Therm. Anal. Calorim., 115 (2014), pp. 1111-1117
21. H. Li, J. Addai-Mensah, J.C. Thomas, A.R. Gerson, **The influence of Al (III) supersaturation and NaOH concentration on the rate of crystallization of Al(OH)3 precursor particles from sodium aluminate solutions,** J. Colloid Interface Sci., 286 (2005), pp. 511-519
22. E. Tiffo, J.B.B. Mbah, P.D.B. Belibi, J.N.Y. Djobo, A. Elimbi, **Physical and mechanical properties of unheated and heated kaolin based-geopolymers with partial replacement of aluminum hydroxide,** Mater. Chem. Phys., 239 (2020) 122103
23. T. Tsuchida, N. Ichikawa, **Mechanochemical phenomena of gibbsite, bayerite and boehmite by grinding,** React. Solid, 7 (1989), pp. 207-217
24. T. Sato, **Thermal decomposition of aluminum hydroxides to alumina,** Thermochim. Acta, 88 (1) (1985), pp. 69-84
25. T. Sato, **The thermal transformation of gelatinous aluminium hydroxide,** Z. Anorg, Allg. Chem., 391 (1972), pp. 167-173
26. R.L. Frost, J. Kristof, J.M. Schmidt, J.T. Kloprogge, **Raman spectroscopy of potassium acetate-intercalated kaolinites at liquid nitrogen temperature,** Spectrochim. Acta: Mol. Biomol. Spectrosc., 57 (3) (2001), pp. 603-609
27. R.L. Frost, S.J. Van Der Gaast, M. Zbik, J.T. Kloprogge, G.N. Paroz, **Birdwood kaolinite: a highly ordered kaolinite that is difficult to intercalate an XRD, SEM and Raman spectroscopic study,** Appl. Clay Sci., 20 (2002), pp. 177-187

28. J.M. Cases, O. Lietard, J. Yvon, Garino, J.F. Delon, **Etude des propriétés cristallochimiques de kaolinites désordonnées,** Bull. Mineral., 105 (1982), pp. 439-455
29. Z. Lei, X. Li, Z. Li, J. Qu, Q. Zhang, J. Huang, H. Li, **Potassium fixation and the separation from sodium through the formation of K-alunite using activated aluminum hydroxide,** Separ. Sci. Technol., 52 (2017), pp. 1862-1868
30. R.L. Frost, D.L. Wain, R. Wills, A. Musemeci, A. Martens, **A thermogravimetric study of the alunites of sodium, potassium and ammonium,** Thermochim. Acta, 443 (1) (2006), pp. 56-61
31. M. Gonon, G. Fantozzi, H. Osmani, M. Hamidouche, M.A. Madjoubi, N. Bouaouadja, K. Loucif, **Etude de la transformation de trois nuances de kaolin en fonction de la température,** Silicates Industriels - Ceramic Science and Technology, 65 (N°11–12) (2000), pp. 119-124
32. M. Chargui, H. Hamidouche, Y. Belhouchet, R. Jorand, G. Doufnoune, Fantozzi, **Mullite fabrication from natural kaolin and aluminum slag,** Boletín Soc. Española Cerámica Vidr., 57 (2018), pp. 169-177
33. F. Sahnoune, M. Chegaar, N. Saheb, P. Goeuriot, F. Valdivieso, **Algerian kaolinite used for mullite formation,** Appl. Clay Sci., 38 (2008), pp. 304-310
34. V. Viswabaskaran, F.D. Gnanam, M. Balasubramanian, **Effect of MgO, Y2O3and boehmite additives on the sintering behavior of mullite formed from kaolinite-reactive alumina,** J. Mater. Process. Technol., 142 (2003), pp. 275-281
35. C.N. Djanganga, E. Kamseu, M. Kor Ndikontar, G.L. Nana, J. Soro, U.C. Melo, A. Elimbi, P. Blanchart, D. Njopwouo, **Sintering behavior of porous ceramic kaolin–corundum composites: phase evolution and densification,** Mater. Sci. Eng., A, 528 (2011), pp. 8311-8318
36. G.M. Brindley, M. Nakahira, **Kaolinite–mullite reaction series: I–III,** J. Am. Ceram. Soc., 42 (7) (1959), pp. 311-324
37. C. N Djangang, A. B Tchamba, E. Kamseu, U.C. Melo, A. Elimbi, A.M. Ferrari, C. Leonelli, **Reaction sintering and microstructural evolution in metakaolin-metastable alumina composites,** J. Therm. Anal. Calorim., 117 (2014), pp. 1035-1045
38. K.C. Liu, G. Thomas, A. Caballero, J.S. Moya, S. Aza, **Mullite formation in kaolinite - α-alumina,** Acta Metall., 42 (1994), pp. 489-495
39. Z. Malou, M. Hamidouche, H. Belhouchet, **Thermal shock resistance of Mullite obtained from Kaolin and tri-hydrated alumina,** High. Temp. - High. Press., 47 (N°2) (2017), pp. 179-190
40. M. Sainz, F. Serrano, J. Amigo, J. Bastida, A. Caballero, **XRD microstructural analysis of mullites obtained from kaolinite–alumina mixtures,** J. Eur. Ceram. Soc., 20 (2000), pp. 403-412
41. N. Bouzidi, **Influence des impuretés des kaolins sur les propriétés des produits de cuisson, PhD** Thesis, Ecole Nationale Supérieure des Mines de Saint-Etienne (2012), in French. <NNT :2012EMSE0660>. <tel-00847400>
42. H.-J. Kleebe, F. Siegelin, T. Straubinger, G. Ziegler, **Conversion of Al_2O_3-SiO_2 powder mixtures to 3:2 mullite following the stable or metastable phase diagram,** J. Eur. Ceram. Soc., 21 (2001), pp. 2521-2533
43. A. Raghdi, M. Heraiz, F. Sahnoune, N. Saheb, **Mullite-zirconia composites prepared from halloysite reaction sintered with boehmite and zirconia,** Appl. Clay Sci., 146 (2017), pp. 70-80
44. P.G. De la Iglesia, O. García-Moreno, J.L. Menéndez, A.H. De Aza, I. Alvarez-Clemares, R. Torrecillas, **Microstructural development and mechanical performance of mullite-alumina and hibonite-alumina ceramics with controlled addition of a glass phase,** Ceram. Int., 44 (Issue 2) (2018), pp. 2292-2299
45. S.M. Naga, A. El-Maghraby, **Preparation and characterization of porous fibrous mullite bodies doped with TiO_2,** Mater. Char., 62 (2011), pp. 174-180